Applied Catalysis B: Environmental 97 (2010) 115–119

Contents lists available at ScienceDirect

Applied Catalysis B: Environmental

journal homepage: www.elsevier.com/locate/apcatb

# Development of a visible-light-responsive rutile rod by site-selective modification of iron(III) ion on {1 1 1} exposed crystal faces

Naoya Murakami, Asami Ono, Misa Nakamura, Toshiki Tsubota, Teruhisa Ohno*

*Department of Applied Chemistry, Faculty of Engineering, Kyushu Institute of Technology, 1-1 Sensuicho, Tobata, Kitakyushu 804-8550, Japan*

ARTICLE INFO

*Article history:*
Received 24 January 2010
Received in revised form 17 March 2010
Accepted 24 March 2010
Available online 30 March 2010

*Keywords:*
Visible-light-responsive photocatalyst
Shape-controlled rutile titanium(IV) oxide
Site-selective modification of metal ion

ABSTRACT

{1 1 1} exposed crystal faces of shape-controlled rutile titanium(IV) oxide ($TiO_2$) were site-selectively modified with trivalent iron(III) ($Fe^{3+}$) ions by utilizing adsorption property of iron(III)/iron(II) ($Fe^{3+}/Fe^{2+}$) ions. The rutile $TiO_2$ with site-selective modification of $Fe^{3+}$ ions showed high photocatalytic activity under visible-light irradiation as a result of separation of redox sites, i.e., oxidation and reduction proceed over $Fe^{3+}$ ions on {1 1 1} faces and the bare $TiO_2$ surface on {1 1 0} faces, respectively. Double-beam photoacoustic spectroscopic analyses suggest that the high activity of $TiO_2$ with site-selective modification of $Fe^{3+}$ ions is attributed to not efficient electron injection from $Fe^{3+}$ ions but efficient reduction by injected electrons on {1 1 0} faces.



## 1. Introduction

Environmental purification by utilization of the self-cleaning effect on a semiconductor photocatalyst has attracted much attention [1,2]. Among the various kinds of semiconductor photocatalyst, titanium(IV) oxide ($TiO_2$) is the most suitable photocatalyst for application of environmental purification from the viewpoint of chemical stability, availability and no toxic properties. However, a $TiO_2$ photocatalyst is inactive under visible-light irradiation because of its wide bandgap energy (3.0 eV for rutile and 3.2 eV for anatase), and thus, ultraviolet (UV) light, the amount of which corresponds to only a small percentage of total solar energy, is essential for photocatalytic reaction over a $TiO_2$ photocatalyst.

Many efforts have been made over the past few decades to improve the visible-light response of a $TiO_2$ photocatalyst by impurity doping [3–8]. However, impurity doping sometimes increases defects in $TiO_2$, which also work as recombination centers and result in decrease of photocatalytic activity [9,10]. Recently, some visible-light-responsive $TiO_2$ photocatalysts have been developed by modification with a metal surface complex that works as a sensitizer for visible light [11–14]. This method has the advantages of simple preparation and no introduction of defects in $TiO_2$. In our previous study, the method was applied to titania nanotubes, the outside/inside surfaces of which were site-selectively modified with metal ions for separation of photocatalytic redox sites [15]. Although its tubular structure enabled site-selective modification with metal ions, diffusion-controlled reaction was inevitable on the inside surface of TNT. Therefore, for further improvement of photocatalytic activity under visible-light irradiation, it is necessary to modify specific sites on $TiO_2$ particles with metal ions.

Utilization of shape-controlled particles with specific exposed crystal faces may be another method for modification at specific sites. It is well known that physical and chemical properties of semiconductor particles strongly depend on exposed crystal faces [16–18]. For example, certain chemical compounds work as shape-control reagents during the nucleation process by preferential adsorption on specific crystal faces [19]. Therefore, site-selective modification of a shape-controlled nanocrystal with metal ions may be possible by preferential properties depending on the crystal surface. Our studies suggest that a redox reaction proceeds preferentially on specific exposed crystal faces of $TiO_2$, i.e., reduction on {1 1 0} and oxidation on {1 1 1} for rutile reduction on {0 1 1} and oxidation on {0 0 1} for anatase [20–22]. This kind of preferential reaction induces site-selective deposition of metal or metal oxide on specific exposed crystal faces under photoexcitation [20–24].

In the present study, we modified shape-controlled rutile $TiO_2$ having specific exposed crystal faces with iron(III) ($Fe^{3+}$) ion. In our previous study, modification of rutile $TiO_2$ with $Fe^{3+}$ ion, which worked as a sensitizer for visible light, greatly improved photocatalytic reaction under visible-light irradiation [25]. Moreover, characteristic adsorption properties of $Fe^{3+}/Fe^{2+}$ ions on $TiO_2$, which are strongly dependent on valence states of iron ions [26], induced site-selective adsorption on the specific exposed crystal faces of rutile $TiO_2$ particles.

* Corresponding author. Tel.: +81 93 884 3318; fax: +81 93 884 3318.
*E-mail address:* tohno@che.kyutech.ac.jp (T. Ohno).

0926-3373/$ – see front matter © 2010 Elsevier B.V. All rights reserved.
doi:10.1016/j.apcatb.2010.03.030

## 2. Experimental

### 2.1. Sample preparation

#### 2.1.1. Preparation of rutile rods

Fifty decimeter cube of aqueous titanium(III) chloride solution (0.15 mol $dm^{-3}$) containing sodium chloride (5 mol $dm^{-3}$) in a Teflon bottle was stirred for 1 h, and then the bottle was sealed with a stainless jacket and heated at 200 °C for 3 h in an oven. After the hydrothermal treatment, the residue in the Teflon bottle was washed with Milli-Q water several times until ionic conductivity was <10 μS $cm^{-1}$. The particles were dried under reduced pressure. In the present study, commercial rutile $TiO_2$ (TAYCA, MT-600B) with 27 $m^2$ $g^{-1}$ of specific surface area was used as a reference sample.

#### 2.1.2. Non-site-selective modification of the entire surface with $Fe^{3+}$ ions

An aqueous suspension composed of samples and an aqueous solution of iron(III) nitrate ($Fe(NO_3)_3$) was stirred for 6 h under an aerated condition. After stirring, the supernatant and residue were separated by filtration, and the residue was washed with deionized water several times until the ionic conductivity of the supernatant was <10 μS $cm^{-2}$ in order to remove $NO_3^-$ ions, and then the particles were dried under reduced pressure.

#### 2.1.3. Site-selective modification of specific exposed faces with $Fe^{3+}$ ions

An aqueous suspension composed of samples and an aqueous solution of $Fe(NO_3)_3$ with and without ethanol was stirred for 6 h under an aerated condition. The stirring was carried out under UV irradiation with a 500-W super-high-pressure mercury lamp (Ushio, SX-UI501UO), the light intensity of which was 1.0 mW $cm^{-2}$. The supernatant and residue were separated by filtration immediately after 6 h of stirring. The residue was washed with deionized water several times until the ionic conductivity of the supernatant was <10 μS $cm^{-1}$, and then the particles were dried under reduced pressure.

### 2.2. Characterization

The crystal structures of the powders were confirmed by using an X-ray diffractometer (Rigaku, MiniFlex II) with Cu Kα radiation (λ = 1.5405 Å). The diffuse reflectance (DR) spectra were measured using a UV–vis spectrophotometer (Shimadzu, UV-2500PC) equipped with an integrating sphere unit (Shimadzu, ISR-240A). The specific surface areas of the particles were determined with a surface area analyzer (Quantachrome, Nova 4200e) by using the Brunauer–Emmett–Teller equation. The morphology of prepared $TiO_2$ particles was observed by using transmission electron microscopy (TEM; Hitachi, H-9000NAR) and scanning electron microscopy (SEM; JEOL, JSM-6701FONO). The net amount of $Fe^{3+}$ ions on the $TiO_2$ surface was estimated by analysis of filtrate with inductively coupled plasma optical emission spectroscopy (ICP-OES; Shimadzu, ICPS-8000). X-ray photoelectron spectra (XPS) of the $TiO_2$ particles were measured using a photoelectron spectrometer (JEOL, JPS90SX) with an Mg Kα source (1253.6 eV). The shift of binding energy was corrected using the C 1s level at 284.6 eV as an internal standard.

### 2.3. Photocatalytic decomposition of acetaldehyde

Photocatalytic activities of samples were evaluated by photocatalytic decomposition over acetaldehyde. One hundred milligrams of powder, which has complete extinction of the incident radiation, was spread on a glass dish, and the glass dish was placed in a 125 $cm^3$ Tedlar bag (AS ONE Co. Ltd.). Five hundred parts per million of gaseous acetaldehyde was injected into the Tedlar bag, and photoirradiation was performed at room temperature after the acetaldehyde had reached an adsorption equilibrium. The gaseous composition in the Tedlar bag was 79% $N_2$, 21% $O_2$, <0.1 ppm of $CO_2$ and 500 ppm of acetaldehyde, and relative humidity was ca. 30%. A light-emitting diode (LED; Lumileds, Luxeon LXHL-NRR8), which emitted light at a wavelength of ca. 455 nm with an intensity of 1.0 mW $cm^{-2}$, was used for visible-light irradiation. The emission spectrum of the LED is shown in Fig. 1. The concentrations of acetaldehyde and carbon dioxide ($CO_2$) were estimated by gas chromatography (Shimadzu, GC-8A, FID detector) with a PEG-20 M 20% Celite 545 packed glass column and gas chromatography (Shimadzu, GC-9A, FID detector) with a TCP 20% Uniport R packed column and a methanizer (GL Sciences, MT-221), respectively.

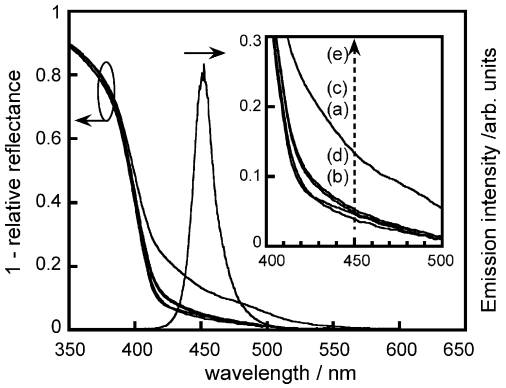


**Fig. 1.** UV–vis spectra of (a) D-01, (b) P-01, (c) PE-01, (d) bare $TiO_2$, and (e) D-032 and emission spectrum of the LED used for photocatalytic evaluation.

### 2.4. Double-beam photoacoustic spectroscopic measurement

A gas-exchangeable photoacoustic (PA) cell equipped with two valves for gas flow was used, and a $TiO_2$ sample was placed in the cell. The atmosphere was controlled by a flow of nitrogen containing ethanol vapor ($N_2$ + EtOH) or artificial air containing ethanol vapor (air + EtOH), and the measurements were conducted after shutting off the valves, i.e., in a closed system at room temperature. An LED emitting light at ca. 625 nm (Lumileds, Luxeon LXHL-ND98) was used as a probe light, and the output intensity was modulated by a digital function generator (NF, DF1905) at 80 Hz. In addition to the modulated light, a blue-LED (Lumileds, Luxeon LXHL-NB98, emitting light at ca. 470 nm, 8.1 mW $cm^{-2}$) was also used as simultaneous continuous irradiation for photoexcitation. The PA signal acquired by a condenser microphone buried in the cell was amplified and monitored by a digital lock-in amplifier (NF, LI5640). Detailed setups of double-beam photoacoustic (DB-PA) spectroscopic measurements have been reported previously [27].

## 3. Results and discussion

### 3.1. Physical and chemical properties of bare and $Fe^{3+}$-modified $TiO_2$ samples

The crystal structure of the sample prepared by hydrothermal treatment of titanium(III) chloride solution in the presence of sodium chloride was attributed to rutile $TiO_2$ without other crystal phases from the XRD pattern. Moreover, SEM, TEM and electron diffraction analyses indicated that the prepared $TiO_2$ has a rod shape with {1 1 0} and {1 1 1} exposed crystal faces. The specific surface area of the bare rutile rod was 34 $m^2$ $g^{-1}$. These results coincide with results of previous studies [21,28,29].

**Table 1**
$Fe^{3+}$-modified $TiO_2$ prepared by different methods and using different samples.

| Name | Sample | $Fe^{3+}$(init), wt% | $Fe^{3+}$(net), wt% | Preparation condition |
|---|---|---|---|---|
| D-004 | Rutile rod | 0.04 | 0.04 | Dark |
| P-004 | Rutile rod | 0.04 | 0.04 | Photo |
| D-01 | Rutile rod | 0.10 | 0.10 | Dark |
| P-01 | Rutile rod | 0.10 | 0.09 | Photo |
| PE-01 | Rutile rod | 0.10 | 0.04 | Photo + EtOH |
| D-032 | Rutile rod | 0.32 | 0.32 | Dark |
| P-032 | Rutile rod | 0.32 | 0.22 | Photo |
| DMT | MT-600B | 0.05 | 0.05 | Dark |
| PEMT | MT-600B | 0.10 | 0.05 | Photo + EtOH |

D, P, and PE in sample names denote preparation condition i.e., under dark, photoirradiation, and photoirradiation in the presece of ethanol, respectively. Number in sample names denote weight ratio of $Fe^{3+}$ ion to $TiO_2$, thus, 004, 01 and 032 mean 0.04, 0.10 and 0.32 wt% of $Fe^{3+}$ ion in starting solutions for $Fe^{3+}$ modification.

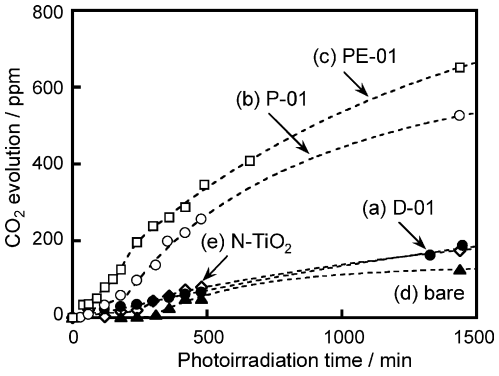


**Fig. 2.** Time courses of $CO_2$ evolution for acetaldehyde decomposition over (a) D-01, (b) P-01, (c) PE-01, (d) bare $TiO_2$, and (e) N-$TiO_2$ under visible-light irradiation.

Table 1 shows $Fe^{3+}$-modified samples prepared by three $Fe^{3+}$-modification methods. The valence state of iron ions on $TiO_2$ particles was confirmed to be a trivalent state by XPS analyses. UV irradiation during $Fe^{3+}$ modification decreased the net amount of $Fe^{3+}$ ions on the $TiO_2$ surface, while almost of $Fe^{3+}$ ion was modified on the $TiO_2$ surface prepared in the dark. It has been reported that $Fe^{2+}$ ions hardly adsorb on the $TiO_2$ surface compared to $Fe^{3+}$ ions [26]. Therefore, it is thought that $Fe^{2+}$ ions were produced as a result of reduction of $Fe^{3+}$ ions by photoexcited electrons in $TiO_2$ and then the produced $Fe^{2+}$ ions desorbed from the $TiO_2$ surface. Addition of ethanol decreased the net amount of $Fe^{3+}$ ions on the surface because reduction of $Fe^{3+}$ ions was accelerated due to an electron accumulation in $TiO_2$, which was induced by efficient hole consumption.

Our previous study suggested that reduction and oxidation on the rutile rod proceed predominantly on {1 1 0} and {1 1 1} exposed crystal faces, respectively [21]. Therefore, $Fe^{3+}$ ions are expected to mainly adsorb on {1 1 1} faces under UV irradiation because $Fe^{3+}$ ions on {1 1 0} faces desorb due to reduction of $Fe^{3+}$ to $Fe^{2+}$ (Scheme 1). The produced $Fe^{2+}$ ions are thought to be recovered

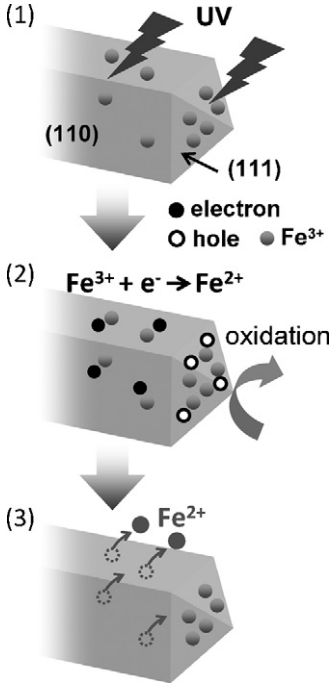


**Scheme 1.** Site-selective modification on a shape-controlled rutile rod with {1 1 0} and {1 1 1} exposed crystal faces.

to $Fe^{3+}$ ions as a result of reoxidation by oxygen and/or positive holes on {1 1 1} faces [30]. Actually, a further decrease in the net amount of $Fe^{3+}$ ions on the surface was observed when the same modification method was used under a deaerated condition.

Modification with $Fe^{3+}$ ions induced a color change form white to pale yellow as reported previously [25]. Fig. 1 shows UV–vis spectra of bare and $Fe^{3+}$-modified $TiO_2$. In the wavelength region between 400 and 500 nm of DR spectra, an upward shift of photoabsorption was observed. Photoabsorption was increased with an increase in the net amount of $Fe^{3+}$ ions on $TiO_2$ prepared by the same modification method. However, relationship between photoabsorption and net amount of modified $Fe^{3+}$ ion was not observed among D-01, P-01 and PE-01. For example, PE-01 exhibited larger absorption than P-01 in spite of smaller net amount of $Fe^{3+}$. This presumably indicate that $Fe^{3+}$ ions on PE-01, which were site-selectively modified on {1 1 1} faces with high density and formed larger cluster of $Fe^{3+}$ compound, resulted in larger photoabsorption. Therefore, not only the amount of $Fe^{3+}$ ions but also density of $Fe^{3+}$ ions has an influence on photoabsorption of $Fe^{3+}$-modified $TiO_2$.

### 3.2. Photocatalytic activity for decomposition of acetaldehyde under visible-light irradiation

Fig. 2 shows the time course of $CO_2$ evolution for decomposition of acetaldehyde under visible-light irradiation. Photocatalytic activity of $Fe^{3+}$-modified $TiO_2$ was higher than that of bare $TiO_2$. This indicated that $Fe^{3+}$ ions on $TiO_2$ induced photocatalytic reaction under visible-light irradiation as follows [25]: (1) photoexcited $Fe^{3+}$ ions injected electrons into $TiO_2$ and $Fe^{3+}$ ions became an oxidized state ($Fe^{4+}$), (2) injected electrons migrated in the bulk and reduced oxygen species on the $TiO_2$ surface and (3) the oxidized state of $Fe^{3+}$ ions ($Fe^{4+}$) oxidized acetaldehyde and returned to the initial state of metal ions ($Fe^{3+}$). PE-01 and P-01 showed higher photocatalytic activity than that of nitrogen-doped $TiO_2$ (N-$TiO_2$; Sumitomo Chemical Co.), which is well known as a conventional visible-light-responsive $TiO_2$. Moreover, photocatalytic activity of $Fe^{3+}$-modified $TiO_2$ showed dependence on its preparation method (PE-01 > P-01 > D-01). There are three possible reasons for the difference in photocatalytic activity: (1) net amount of $Fe^{3+}$ on $TiO_2$, (2) structure of $Fe^{3+}$ species depending on the modification condition and (3) site selectivity of $Fe^{3+}$ modification. The following experiments were carried out to clarify the reason.

Fig. 3 shows dependence of the net amount of $Fe^{3+}$ ions on photocatalytic activity ($CO_2$ evolution at 240 min of photoirradiation). Photocatalytic activity was increased by a small amount of $Fe^{3+}$ modification because of the increase in visible-light photoabsorption. On the other hand, an excess amount of $Fe^{3+}$ modification decreased photocatalytic activity, presumably due to a decrease of

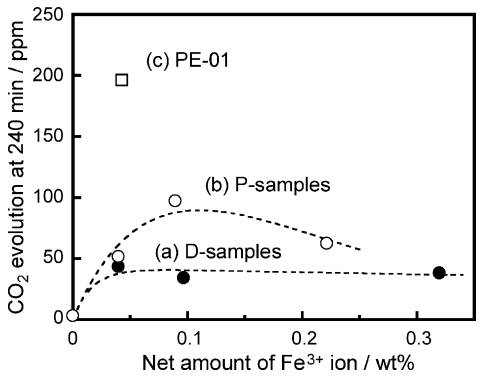


**Fig. 3.** $CO_2$ evolution at 240 min of photoirradiation for photocatalytic decomposition over (a) D-samples, (b) P-samples, and (c) PE-01 as a function of net amount of $Fe^{3+}$ ions.

reduction sites by coverage of the $TiO_2$ surface and/or formation of inactive aggregated $Fe^{3+}$ species. Therefore, increase in photocatalytic activity of an $Fe^{3+}$-modified rutile nanorod prepared by UV irradiation might be attributable to the removal of an excess amount of $Fe^{3+}$ because UV irradiation decreased the net amount of $Fe^{3+}$ ions as indicated in Table 1. However, this hypothesis is denied by the different dependence of photocatalytic activity on the net amount of $Fe^{3+}$ ions of a non-site-selective $Fe^{3+}$-modified rutile nanorod as indicated in Fig. 3. Thus, high photocatalytic activity of an $Fe^{3+}$-modified rutile nanorod prepared by UV irradiation was not attributed to removal of an excess amount of $Fe^{3+}$ ions.

The same modification method was applied to commercial rutile $TiO_2$ particles, which have a spherical shape without specific exposed crystal faces. UV irradiation during $Fe^{3+}$ modification is thought to induce no site-selective modification on the particle because a redox reaction proceeds in the neighboring sites without being separated. Fig. 4 shows the time course of $CO_2$ evolution for decomposition of acetaldehyde over $Fe^{3+}$-modified commercial rutile under visible-light irradiation. These two samples were prepared by different modification methods, but the net amounts of $Fe^{3+}$ ions were modified on these samples by adjusting the initial amount of $Fe^{3+}$. A large difference in photocatalytic reaction was not observed, regardless of the presence or absence of UV irradiation during $Fe^{3+}$ modification. This indicates that the UV irradiation induced formation of the same $Fe^{3+}$ species for photocatalytic reaction as that prepared in the dark. Therefore, the reason for the high activity of P- and PE-samples is that UV irradiation during $Fe^{3+}$ modification induces site-selective modification with $Fe^{3+}$ ions.

An excess amount of $Fe^{3+}$ modification decreased photocatalytic activity even for P-samples because it deteriorated site-selective modification of {1 1 1} faces and induced modification of {1 1 0} faces with $Fe^{3+}$ ions. Moreover, D-samples showed lower photocatalytic activity than that of DMT (Figs. 2 and 4). This indicates that modification of {1 1 0} faces decreases photocatalytic activity because efficient reduction on {1 1 0} faces was retarded due to coverage of $Fe^{3+}$ ions.

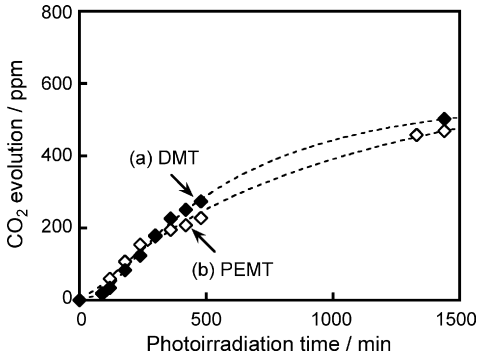


**Fig. 4.** Time courses of $CO_2$ evolution for acetaldehyde decomposition over (a) DMT and (b) PEMT under visible-light irradiation.

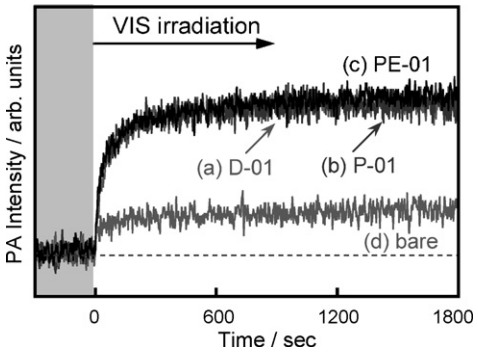


**Fig. 5.** Time-course curves of PA signals of (a) D-01, (b) P-01, (c) PE-01, and (d) bare $TiO_2$ under visible-light irradiation in the presence of $N_2$ + EtOH.

### 3.3. PA spectroscopic detection of electron behavior under visible-light irradiation

The behavior of electrons injected into $TiO_2$ was observed by DB-PAS [27]. Fig. 5 shows time-course curves of PA intensity for D-01, P-01, PE-01 and bare $TiO_2$ under visible-light irradiation in the presence of $N_2$ + EtOH. PA intensity increased with visible-light irradiation because $Ti^{4+}$ was reduced to $Ti^{3+}$ by injected electrons from photoexcited $Fe^{3+}$ ions. Thus, increase in PA intensity is attributed to the amount of injected electrons. The saturation limit of PA intensity showed no dependence on $Fe^{3+}$ modification method. This result is reasonable because photoabsorption of these samples was not so different. This indicates that the main factor of high photocatalytic activity was not oxidation on oxidized $Fe^{3+}$ ($Fe^{4+}$) generated by electron injection from $Fe^{3+}$ ions into $TiO_2$. Another plausible factor is efficiency of reduction on a rutile $TiO_2$ nanorod modified with $Fe^{3+}$ by injected electrons.

DB-PA measurements in the presence of oxygen were also carried out in order to estimate efficiency of reduction by injected electrons. Fig. 6 shows time-course curves of PA intensity for D-01, P-01, PE-01 and bare $TiO_2$ under visible-light irradiation in the presence of air + EtOH. PA intensity attributed to $Ti^{3+}$ formation was greatly decreased because electron accumulation was retarded due to electron consumption by oxygen species on the $TiO_2$ surface. Steady-state value of PA intensity showed dependence on modification method (D-01 > P-01 > PE-01), and site selectivity of $Fe^{3+}$ modification induced smaller PA intensity. This suggests that reduction proceeds more efficiently on the surfaces of P-01 and

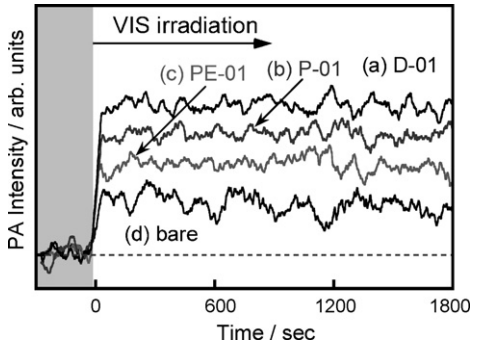


**Fig. 6.** Time-course curves of PA signals with 50 points smoothing of (a) D-01, (b) P-01, (c) PE-01, and (d) bare $TiO_2$ under visible-light irradiation in the presence of air + EtOH.

PE-01 than on the surfaces of D-01 because efficient reduction of oxygen on {1 1 0} faces proceeded without retardation by coverage of $Fe^{3+}$ ion.

## 4. Conclusion

UV irradiation during $Fe^{3+}$-modification on shape-controlled rutile rod induced high photocatalytic activity under visible-light irradiation because {1 1 1} exposed crystal faces were site-selectively modified with $Fe^{3+}$ ions and redox reactions were spatially separated. On the other hand, photocatalytic activity of non-site-selectively modified $TiO_2$ was low. DB-PA analyses indicated that photocatalytic activity was determined not by efficiency of electron injection but by efficiency of reduction by injected electrons. The efficiency of reduction was influenced by site-selectivity of $Fe^{3+}$-modification on {1 1 1} faces because $Fe^{3+}$ ions on {1 1 0} faces retard efficient reduction on the bare $TiO_2$ surface.

## Acknowledgements

This work was supported by a grant of Knowledge Cluster Initiative implemented by the Ministry of Education, Culture, Sports, Science and Technology (MEXT) and the New Energy and Industrial Technology Development Organization (NEDO).

## References

[1] A. Fujishima, T.N. Rao, D.A. Tryk, J. Photochem. Photobiol. C: Photochem. Rev. 1 (2000) 79.
[2] M.R. Hoffmann, S.T. Martin, W. Choi, D.W. Bahnemann, Chem. Rev. 95 (1995) 69–96.
[3] S. Sato, Chem. Phys. Lett. 123 (1986) 126.
[4] R. Asahi, T. Morikawa, T. Ohwaki, K. Aoki, Y. Taga, Science 293 (2001) 269.
[5] T. Umebayashi, T. Yamaki, H. Itoh, K. Asai, Appl. Phys. Lett. 81 (2002) 454.
[6] T. Ohno, M. Akiyoshi, T. Umebayashi, K. Asai, T. Mitsui, M. Matsumura, Appl. Catal. A: Gen. 265 (2004) 115.
[7] T. Ohno, T. Tsubota, K. Nishijima, Z. Miyamoto, Chem. Lett. 33 (2004) 750.
[8] H. Irie, Y. Watanabe, K. Hashimoto, Chem. Lett. 32 (2003) 772.
[9] N. Serpone, D. Lawless, Langmuir 10 (1994) 643.
[10] S. Ikeda, N. Sugiyama, B. Pal, G. Marci, L. Palmisano, H. Noguchi, K. Uosaki, B. Ohtani, Phys. Chem. Chem. Phys. 3 (2001) 267.
[11] H. Kisch, L. Zang, C. Lange, W.F. Maier, C. Antonius, D. Meissner, Angew. Chem. Int. Ed. 37 (1998) 3034.
[12] L. Zang, C. Lange, I. Abraham, S. Storck, W.F. Maier, H. Kisch, J. Phys. Chem. B 102 (1998) 10765.
[13] L. Zang, W. Macyk, C. Lange, W.F. Maier, C. Antonius, D. Meissner, H. Kisch, Chem. Eur. J. 6 (2000) 379.
[14] W. Macyk, H. Kisch, Chem. Eur. J. 7 (2001) 1862.
[15] N. Murakami, Y. Fujisawa, T. Tsubota, T. Ohno, Appl. Catal. B: Environ. 92 (2009) 56.
[16] P.A. Morris Hotsenpiller, J.D. Bolt, W.E. Farneth, J.B. Lowekamp, G.S. Rohrer, J. Phys. Chem. B 102 (1998) 3216.
[17] J.B. Lowekamp, G.S. Rohrer, P.A. Morris Hotsenpiller, J.D. Bolt, W.E. Farneth, J. Phys. Chem. B 102 (1998) 7323.
[18] A. Imanishi, H. Suzuki, K. Murakoshi, Y. Nakato, J. Phys. Chem. B 110 (2006) 21050.
[19] C.G. Read, E.M.P. Steinmiller, K. Choi, J. Am. Chem. Soc. 131 (2009) 12040.
[20] T. Ohno, K. Sarukawa, M. Matsumura, New J. Chem. 26 (2002) 1167.
[21] E. Bae, N. Murakami, T. Ohno, J. Mol. Catal. A: Chem. 300 (2009) 72.
[22] N. Murakami, Y. Kurihara, T. Tsubota, T. Ohno, J. Phys. Chem. C 113 (2009) 3062.
[23] H. Kato, K. Asakura, A. Kudo, J. Am. Chem. Soc. 125 (2003) 3082.
[24] Y. Matsumoto, S. Ida, T. Inoue, J. Phys. Chem. C 112 (2008) 11614.
[25] N. Murakami, T. Chiyoya, T. Tsubota, T. Ohno, Appl. Catal. A: Gen. 348 (2008) 148.
[26] T. Ohno, D. Haga, K. Fujihara, K. Kaizaki, M. Matsumura, J. Phys. Chem. B 101 (1997) 6415.
[27] N. Murakami, O.O.P. Mahaney, R. Abe, T. Torimoto, B. Ohtani, J. Phys. Chem. C 111 (2007) 11927–11935.
[28] E. Hosono, S. Fujihara, K. Kakiuchi, K. Imai, J. Am. Chem. Soc. 126 (2004) 7790.
[29] K. Kakiuchi, E. Hosono, H. Imai, T. Kimura, S. Fujihara, J. Cryst. Growth 293 (2006) 541.
[30] W. Choi, A. Termin, M.R. Hoffmann, J. Phys. Chem. B 98 (1994) 13669.